7-1-2023

Uncertainty in overturning of precariously balanced rocks due to basal contact

M. Khalid Saifullah
University of Nebraska-Lincoln

Christine E. Wittich
University of Nebraska - Lincoln, cwittich@unl.edu

Received: 23 February 2023 | Revised: 29 June 2023 | Accepted: 1 July 2023

DOI: 10.1002/eqe.3970

RESEARCH ARTICLE

WILEY

Uncertainty in overturning of precariously balanced rocks due to basal contact

M. Khalid Saifullah | **Christine E. Wittich**

Department of Civil and Environmental Engineering, University of Nebraska-Lincoln, Lincoln, Nebraska, USA

Correspondence
Christine E. Wittich, Department of Civil and Environmental Engineering, University of Nebraska-Lincoln, Lincoln, NE, USA.
Email: cwittich@unl.edu

Funding information
Southern California Earthquake Center, Grant/Award Number: #20106; Pacific Gas and Electric Company

Abstract

Precariously balanced rocks (PBRs) are a type of naturally occurring freestanding structure that provides valuable information to constrain seismic hazard at return periods which are important for critical facilities such as nuclear power plants and nuclear repositories. Exposure ages have been established to be in excess of 10,000–30,000 years, which is why precarious rocks are one of the only available means to validate seismic hazard associated with long return periods. One critical component for constraining seismic hazard in this way is the overturning estimate of a given precarious rock as a function of earthquake intensity. However, current state-of-the-art methods for modeling the seismic response of precarious rocks involve significant sources of uncertainty. One of the main sources of uncertainty stems from the interface of the rock, which is usually occluded during surveying and assumed during modeling. Through extensive shake table testing, this study analyzes the uncertainty in the overturning response of a granite precarious rock specimen incorporating various degrees of interface contact. The results indicate that a small variation in the contact geometry could result in a substantial increase in the stability of the specimen, which is significant given the difficulty of surveying the interface of PBRs in the field. Repeatability tests indicate that the overturning demand can vary up to nearly ±50%. The probabilistic overturning responses are compared across the interface changes to bound uncertainty; and, the effect of modeling parameters, namely the contact normal stiffness, is evaluated through a parametric study and comparison with experimental results.

KEYWORDS
distinct element modeling, freestanding structures, precariously balanced rocks, rocking, seismic hazard, shake table testing

Novelty

- This study presents shake table testing and distinct element modeling of precariously balanced rocks (PBRs) for the first time.
- Small variations in the interface geometry can significantly impact the stability, which is significant given the difficulty of surveying the interface of these rocks.
- Repeatability tests indicate that the overturning demand can vary up to 50% over a range of ground motion characteristics.
- Distinct element models are recommended to utilize normal stiffnesses within the range of 5–15 GPa/m, beyond which the predictions diverge from the experimental baseline.

1 | INTRODUCTION

Precariously balanced rocks (PBRs) are a type of natural freestanding structures, which have been in existence for tens of thousands of years. Their precariousness serves as an indicator of the maximum ground motion that could have taken place at their location. As such, these structures are vital in the fields of seismology and civil engineering, specifically in seismic hazard analysis. Nonetheless, predicting the seismic response of freestanding structures currently presents significant uncertainties, mainly attributable to geometrical, interface conditions, material, and ground motion characteristics. Geometric and model simplifications exacerbate this uncertainty, although simplifications are frequently employed in the modeling of these complex structures.

Housner's[1] early work on the behavior of inverted pendulum-type structures sheds light on the rocking response of rigid freestanding blocks. In his work, the classical rigid body rocking problem is modeled with a freestanding structure as a simplified 2D projection of a rectangular rocking block, symmetric about its center of mass, incorporating several assumptions including friction at the interface that is high enough to produce a pure rocking response. Over the last few decades since this work, a substantial number of studies explored the response of freestanding structures with different variations and assumptions. Yim et al.[2] further explored this rocking system and concluded that the rocking behavior is extremely sensitive to small changes in size and slenderness of the block as well as the ground motion characteristics. While this sensitivity was significant on a motion-by-motion basis, trends emerged when the problem was cast in a probabilistic formulation. The probabilistic trends drawn from their study revealed that the overturning stability increases with an increase in block size and a decrease in slenderness, while the stability decreases with the increasing ground motion intensity. Moreover, low repeatability is also revealed when the single block rocking problem is studied experimentally,[3] thus, adding another dimension to the uncertainty.

While many studies have treated the freestanding block as a rigid block rocking on a rigid foundation, extensions to the classical model have been proposed and analyzed to understand the response of more realistic systems. For example, Psycharis and Jennings[4] studied a rigid block rocking on a flexible foundation by employing two different modeling approaches, a two-spring foundation, and a Winkler foundation. Similar to previous studies, the nonlinearity and the sensitivity of the rocking problem were revealed in the behavior. In addition, many researchers have recognized that pure rocking behavior alone may be insufficient to illustrate the seismic response of many systems, where sliding is also a key mode in the overall behavior. Keeping in consideration this realistic observation, Ishiyama[5] concluded that the earthquake response of a simple two-dimensional single block rectangular rigid body resting on a rigid floor should be defined by six different rigid body modes: rest, slide, rotation, slide rotation, translation jump, and rotation jump. With the exception of a point-impact assumption instead of planar impact, Shenton and Jones[6] adopted a similar characterization of response by using five similar modes—namely rest, slide, rock, slide-rock, and free-flight mode, in which the free-flight mode encompassed both the translation jump and rotation jump of Ishiyama.[5] When the single block problem is cast into three dimensions with an analytical approach, even the simple rocking problem with point contacts becomes increasingly complex, as demonstrated by Konstantinidis and Makris.[7] However, the analytical study by Chatzis and Smyth[8] indicates that the 2D modeling of freestanding structures is not a solution for 3D problems. Therefore, numerical techniques such as the distinct element method are often leveraged to study 3D problems with fewer assumptions and simplifications, as

successfully implemented by Papantonopoulos et al.,[9] Psycharis et al.,[10] Ambraseys and Psycharis,[11] and more recently by Saifullah and Wittich.[12]

Experimental studies of Peña et al.[3] and Mouzakis et al.[13] shed light on the low repeatability and sensitivity of these structures due to ground motion and frequency content. Furthermore, Yim et al.[2] have emphasized to study the results of these structures in probabilistic format as it can reveal critical information regarding the trends in results, which are not apparent in a deterministic domain. In addition, the experimental work of Mathey et al.[14] and ElGawady et al.[15] highlight the role of imperfections and interface material, respectively, toward the seismic response of these structures. In the context of PBRs, Purvance et al.[16] compared shake table test results of symmetric and asymmetric freestanding blocks with the corresponding fragilities of these blocks obtained through the classical two-dimensional (Housner[1]) model. Peak ground velocity normalized with peak ground acceleration (i.e., PGV/PGA) is found to be one of the best intensity measures that is predictive of overturning. Although their study shows that the shake table responses of symmetric and asymmetric blocks with simple basal contacts lie within the prediction interval sought through classical model, they pointed out that the classical model overestimates the stability of the structures with complex basal contacts (such as granite boulders). This not only emphasizes the need to use three-dimensional numerical modeling techniques, which are able to capture the complex response, but also the importance of the complexity of the base which is often ignored in the analysis procedure.

Given that several sources of uncertainty have been identified in the seismic response of freestanding structures, there is a distinct need to explore the impact of this uncertainty on the predictions for PBRs. This is compounded by the known sensitivity of the response to interface, or basal, conditions of the rock, where this interface is typically occluded during field surveying and approximating in modeling (Wittich et al.[17]). Therefore, this study aims to explore the uncertainty on the response brought by physical and numerical interface parameters, including the impact of small changes in the interface geometry to reflect that this is typically not known precisely. This is achieved through an extensive shake table testing campaign on realistic granite boulders followed by complementary three-dimensional numerical modeling via DEM. This paper first introduces the suite of ground motions that are utilized in both the shake table testing and the numerical modeling. Then, the shake table testing program is introduced followed by a discussion of the experimental results. This is followed by an overview of the DEM approach and validation of the numerical model.

2 | GROUND MOTIONS

As previously mentioned, this study presents the results of both full-scale shake table testing and a complementary numerical study. Given that both of these approaches rely upon a large database of input earthquake excitations, motion selection is described in detail in this section. The ground motions are primarily acquired from Pacific Earthquake Engineering Research Center (PEER)'s NGA West2 database (Ancheta et al.[18]) with a smaller number from the Center for Engineering Strong Motion Data (CESMD[19]). While the motions originated from these databases, final motion selection and all analyses in this study consider the actual motion of the shake table given these input signals. The ground motion selection is based on the vector intensity measure consisting of peak ground acceleration (PGA) and the ratio of peak ground velocity to peak ground acceleration (PGV/PGA). This vector intensity measure has been shown to be predictive of overturning in past studies, including that of Purvance[20] and Dimitrakopoulos and Paraskeva.[21] While this intensity measure is adopted within this study, its predictive abilities are acknowledged to be limited and a strong predictor of overturning for ground motions is not yet known. Given that PGAis a scalable quantity, the main criterion for selection is adopted to be PGV/PGA. The motions are selected to cover a wide range of PGV/PGA, which are then scaled to different levels of PGA to get sufficient spread in PGV/PGA and PGA space.

While motions were initially selected based upon PGV/PGA of the recorded earthquake motions, final motion selection considered the motions as achieved on the shake table. The achieved motions considered the actual mass of the experimental specimens, but the specimens were rigidly attached to the shake table. This is done to prevent impacts on the shake table due to rocking, which contaminates the recorded acceleration by introducing acceleration spikes. The acceleration spikes were short-lived but resulted in variations to PGA and PGV/PGA. For this reason, experimental results and numerical simulations consider the achieved motions based on the rigidly attached specimen. These achieved motions are presented in Figure 1. The intensity measures obtained from the shake table output are shown as a scatter plot in PGA versus PGV/PGA space and also as response spectra in Figure 1A,B, respectively. As shown, 582 ground motions were selected and represent a wide spread across the intensity measure space and in frequency content.

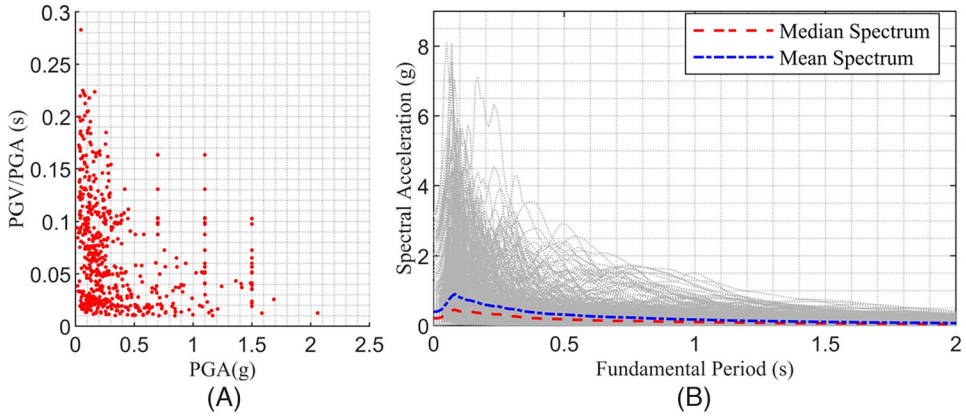

FIGURE 1 Characteristics of the achieved motions on the shake table: (A) PGA versus PGV/PGA and (B) spectral acceleration.

TABLE 1 Test matrix for shake table testing.

Specimen	Number of earthquake tests	Description
SP1	582 (not including repeatability)	Baseline specimen
SP2	582 (not including repeatability)	Chiseled interface of SP1

3 | SHAKE TABLE TESTING

The interface, or basal, condition of the PBR is one of the critical factors that brings about substantial uncertainty in the seismic response of PBRs. It is imperative to analyze this factor physically through experimental investigation involving an actual rock specimen with complex basal contact. To better understand this uncertainty and to reflect the occlusion and approximation of the interface associated with PBR field surveying and modeling, the same rock is evaluated with small variations of its interface geometry. To this end, a granite rock specimen (taken as a representative PBR) was tested under a large set of ground motions (mentioned in Section 2) on a shake table. This specimen is referred to herein as SP1. Small variations were introduced at the base of the rock after the first round of testing through chiseling at the points of contact, and the specimen is tested again under the same set of ground motions. This specimen is referred to herein as SP2. The test matrix is shown in Table 1, where each specimen was subject to a total of 582 earthquake excitations including an extensive investigation of repeatability. The results of this shake table testing campaign are analyzed both deterministically and probabilistically. The following sub-sections outline the experimental setup, specimen characterization, and the results and discussion.

3.1 | Experimental program and physical setup

The experimental investigation is carried out using the University of Nebraska-Lincoln's 7 ft × 7 ft shake table, which can support a payload of 2 tons at 1 g. A large set of historical ground motions are utilized to ensure a sufficient spread of PGV/PGA, as described in Section 2. The selected ground motions are scaled to different PGA levels ranging from 0.01 to 1.5 g to attain adequate intensity measure spread in vector space (see Figure 1A). Though the shake table has 12 inches of stroke in both orthogonal translational directions (bi-directional capabilities), only unidirectional excitation is used for the experimental protocol. It is also important to mention that due to the limited stroke of the shake table, very high values of PGV/PGA along with high PGA are not possible. Owing to the fact that the shake table cannot produce the input ground motions precisely, the achieved (measured) motion of the shake table was used in final motion selection and is presented in Figure 1.

A granite rock specimen weighing 780 lbs. and consisting of highly complex geometry is used as the test specimen in the experimentation process (Figure 2). As real PBRs cannot be removed for dynamic testing, the specimen is used as a representation of a PBR. While the geometry of the specimen was irregular, its footprint was approximately 0.30 m in width by 0.64 m in length with a height of 0.8 m. As the geometry of the interface is a source of uncertainty for PBRs, this is

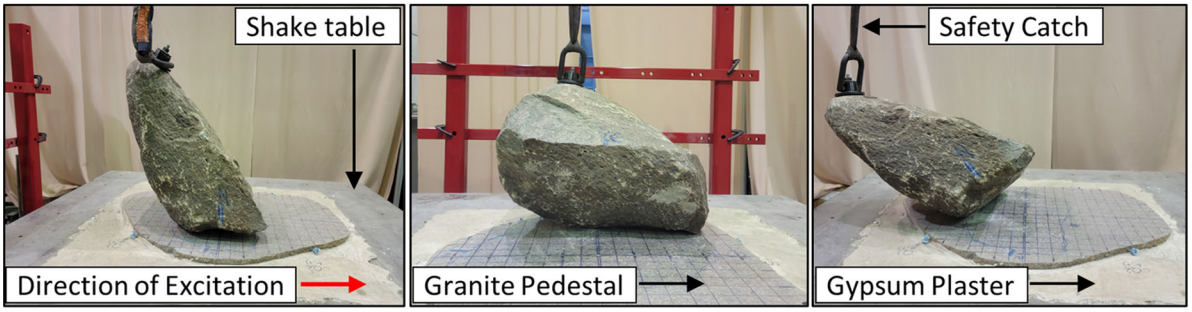

FIGURE 2 Experimental setup.

an explicit variable in this experimentation. Specifically, the base of the rock specimen is chiseled resulting in two different specimens: the baseline, original, or unchiseled specimen (SP1) and the chiseled specimen (SP2). This chiseling is done such that the perimeter of apparent contact is maintained, but the interior contact points are smoothed. This reflects the uncertainty of PBR surveying, which often involves manual surveying of the interface without lifting of the rock (Wittich et al.[17]). The achieved geometric variations are described in detail in the next sub-section on geometric data acquisition.

In order to emulate the field conditions, an unpolished granite slab with natural finish is used as a pedestal on which the specimen is placed to form a granite-granite contact. The granite pedestal is fixed to the shake table by using hydro-stone gypsum plaster to prevent any motion of the pedestal relative to the shake table (Figure 2C). During the experimentation, the rock specimen was free to rotate and translate atop the granite pedestal. The rock specimen was held by a safety catch that ensures sufficient slack to allow for the overturning of the rock but avoids the impact of the rock on the table and, in turn, minimizes the resulting accumulated deterioration of rock material during a large number of tests. While the rock specimen was free to rotate and translate atop the pedestal, no appreciable translation (sliding) was observed throughout the testing and friction was not directly evaluated. While the slab was largely uniform, the rock specimen was placed in the same location for each test so that the angle of excitation remains the same throughout the experimentation. For each test, the binary overturning behavior is noted, the motion of the specimen is recorded by video, and photographs of the final position are collected. A sub-set of the tests explored the issue of repeatability. To track subtle changes in the movement of the structure during the repeatability tests, a vision-based system involving infrared markers was used to acquire the displacement of the structure during each test. The NDI Optotrak Certus system was used for this purpose, which possesses the ability to measure the rigid body displacements of three-dimensional targets with millimeter accuracy.

3.2 | Geometric data acquisition and interface evolution

Geometric data acquisition of the experimental specimen is conducted via LiDAR (Light Detection and Ranging), or laser scanning, with a FARO Focus x130. This is necessary to both aid in the generation of the numerical model, as well as to track the evolution of the interface or base of the rock which may deteriorate due to repeated testing. The geometry of the rock is obtained in the form of a point cloud, which contains the x, y, and z coordinates of the rock's visible geometry. The geometric data acquisition is realized at a very high resolution to capture the rock's geometry at millimeter level.

Scans of the rock base, or interface, are taken throughout testing to aid in tracking the evolution of the interface and to quantify the difference between the two specimens, unchiseled (SP1) and chiseled (SP2). To this end, change detection analysis, which compares point clouds and quantifies differences, is conducted. Considering the two specimens, the change detection analysis is based on the comparison between one scan of the base of the rock in its unchiseled state and another scan of the base in its chiseled state, with the unchiseled scan serving as the reference. Considering the evolution of the specimens, the change detection analysis utilizes the scan prior to shake table testing as the reference. These analyses were conducted in CloudCompare,[22] which measures the cloud-to-cloud absolute distances by using a quadratic local model based on the 10 nearest neighbors. A quadratic local model is preferred in place of the direct nearest neighbor distance between point clouds as it is more versatile and gives a better estimation of the actual surface of the rock

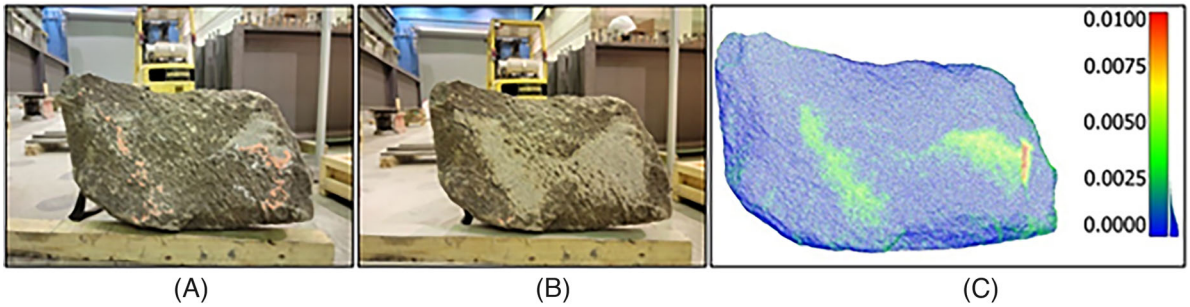

FIGURE 3 Evolution of interface. (A) Unchiseled specimen (SP1), (B) chiseled specimen (SP2), and (C) change detection using point clouds of SP2 and SP1 (in meters).

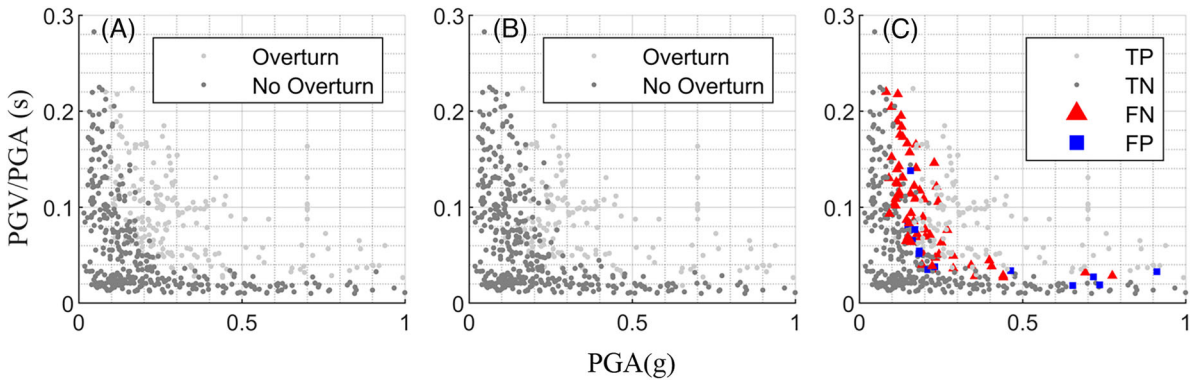

FIGURE 4 Raw shake table results. (A) SP1, (B) SP2, and (C) changes in SP2 with respect to SP1.

(CloudCompare[22]). It is noted that differences less than 1 mm are not able to be reliably detected due to the resolution of the point clouds with respect to the change detection algorithm.

Figure 3 shows the base of the unchiseled specimen (SP1), the chiseled specimen (SP2), and the results of change detection comparing the two point clouds. As evident from Figure 3C, the maximum material that is removed during chiseling is 8 to 10 mm (scale in Figure 3C is in meters) and is localized to one particular area, while on average the material removed in other regions is 3 to 5 mm (green to yellow regions). These changes resulted in SP2 having larger areas in contact at its base compared to SP1. Change detection analysis for the unchiseled (SP1) and chiseled (SP2) specimens throughout their testing yields only negligible differences, which indicates that the granite interface did not deteriorate appreciably throughout the course of hundreds of earthquake motions. While the rock specimen can be considered full-scale, there is a wide range of sizes that can be encountered for PBRs. Larger stresses would be expected at the interface of larger rocks, and so interface deterioration may still occur for larger granitic rocks.

3.3 | Results and discussions

A total of 1164 earthquake tests were conducted, which consists of 582 tests for each specimen. The raw overturning results are presented in Figure 4 in a vector intensity space. Figure 4A,B shows the overturning (light gray) and non-overturning (dark gray) cases for SP1 and SP2 respectively, while Figure 4C shows the agreement between SP1 and SP2 with SP1 taken as the benchmark. The legend in Figure 4C depicts the agreement of Overturning (true positive, TP), agreement of no overturning (True Negative, TN), disagreement of SP2 with respect to SP1 overturning (false negative, FN), and disagreement of SP2 with respect to SP1 non-overturning (false positive, FP). It is evident that the relatively small amount of chiseling at the interface has resulted in increased stability (i.e., higher number of instances of no overturn (NO) in Figure 4B compared to Figure 4A, as also seen by the presence of false negatives [FN] in Figure 4C). Although a small number of cases can be seen where SP2 overturns while SP1 does not (false positives [FP] in Figure 4C), the overall trend indicates

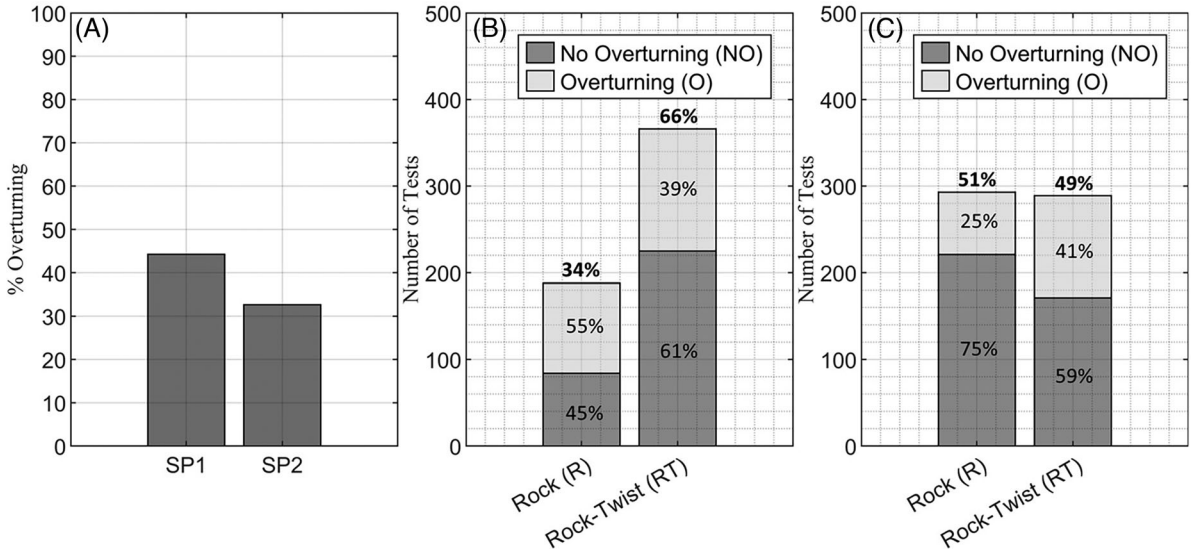

FIGURE 5 Analysis of experimental data. (A) Percentage of overturning cases, (B) dominant modes SP1, and (C) dominant modes SP2.

more stability for SP2 in general. While this is only presented for a single rock, this indicates that assumptions of interface geometry in the field are likely to result in nonconservative overturning estimates.

Figure 5 shows the percentage of tests resulting in overturning for SP1 and SP2, which is 44.2% in 33.6%, respectively, which again highlights the increase in stability (reduction if overturning) due to the chiseled interface. To gain insight into the cause of the increased stability of SP2 compared to SP1, videos taken during each test are analyzed and the dominant response modes are noted. Given that additional instrumentation was not included to track the rigid body motion during these tests, the dominant mode classification was done manually, and two modes were observed: rock and rock-twist. These modes are differentiated by the accumulation of twist or rotation about the specimen's vertical axis. If any appreciable twist was observed, the test was classified as rock-twist. Otherwise, the test would be classified as rocking. It is clarified that sliding was not observed in any test. Figure 5B,C present the dominant modes of both specimens, rocking (R) and rock-twist (RT). For SP1 (Figure 5B), 34% of all tests are dominated by rocking responses, while 66% are rock-twist dominant. In contrast, SP2's overall response is 51% rocking dominant and 49% rock-twist dominant. For SP1, within rocking (R) mode, 45% of cases are no overturning (NO) and 55% are overturning (O), while within rock-twist (RT) mode, 61% are no overturning (NO) and 39% are overturning (O). In comparison, for SP2, within rocking (R) mode, 75% cases are no overturning (NO) and 25% are overturning (O), whereas 59% are no overturning (NO) and 41% are overturning (O) within the rock-twist (RT) mode. This shows that the interface change from SP1 to SP2 partially diminished the rock's tendency to twist. This is logical given that the chiseling smoothed and removed asperities and point contacts, which would contribute to the complex three-dimensional response. In addition, the mode that tends to result in overturning changed as a result of the interface chiseling (from SP1 to SP2). That is, SP1's rocking responses typically resulted in overturning (55%), while SP2's rocking responses typically resulted non-overturning (75%). This is, in part, due to the reduction in overall overturning from SP1 to SP2, but is also indicative of the likely increase in energy dissipation of SP2 compared to SP1 due to the larger contact areas.

While a large difference was noted between the specimens for overturning via rocking mode, the distribution of overturning and non-overturning cases via rock-twist is very similar. As a result, the RT modes shown in Figure 5 are further analyzed in Figure 6 by subclassifying them into slight RT and substantial RT modes. While quantitative sub-classification of modes is not possible, the tests were classified by a single person trained upon group consensus to reduce subjectivity. Slight RT responses do not appear to twist during the dynamic response, but are only able to be determined by comparing the start and end positions. This is estimated at approximately 1° of twist, based upon manual measurements at the end of specific motions. Substantial RT responses show clear twisting behavior during the dynamic response itself. While not a strict threshold, these responses tend to have twisting greater than 1°.

As shown in Figure 6, SP1 rock-twist (RT) response is comprised of 18% slight RT with overturning (O), 30% slight RT with no overturning (NO), 20% substantial RT with overturning (O), 32% substantial RT with no overturning (NO). However, there is a shift in rock-twist (RT) modes from substantial RT to slight RT in SP2 with the response consisting of

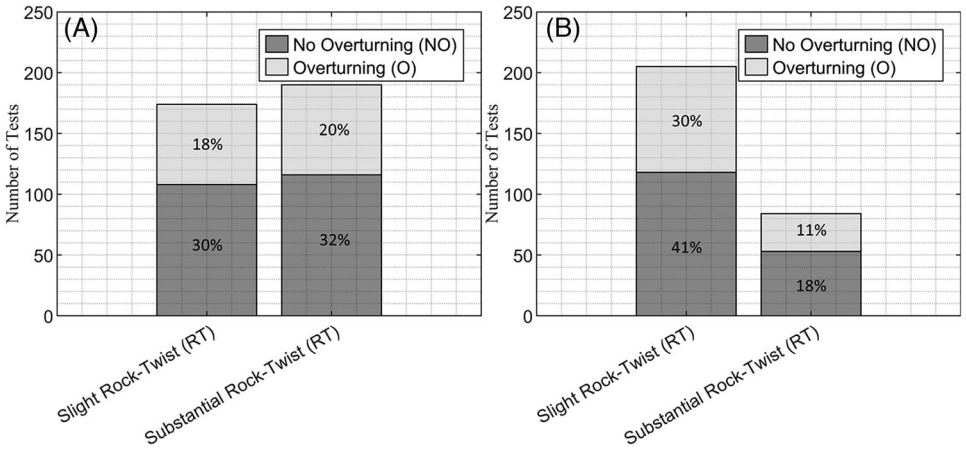

FIGURE 6 Discretization of rock-twist mode (A) SP1 and (B) SP2.

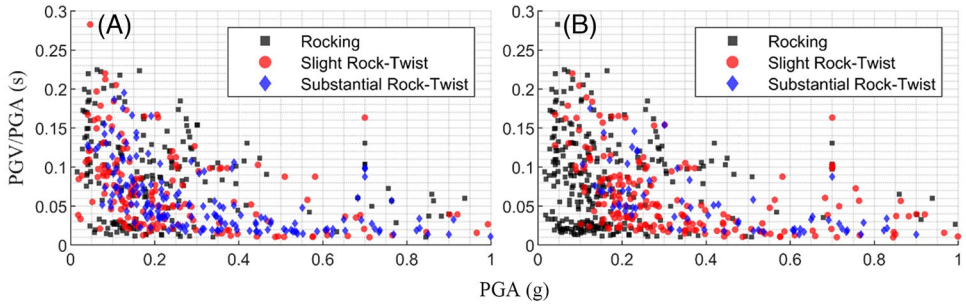

FIGURE 7 Distribution of modes in vector intensity space (A) SP1 and (B) SP2.

30% slight RT with overturning (O), 41% slight RT with no overturning (NO), 11% substantial RT with overturning (O), 18% substantial RT with no overturning (NO). These results shed further light on the modal change between SP1 and SP2. As shown in Figure 5, SP1 is dominated by rock-twist responses, while SP2 had a more even distribution between rock and rock-twist. Further analysis of the rock-twist modes in Figure 6, which discretized the modes into slight and substantial, shows that SP2's rock-twist modes were predominantly only slight rock-twist. Therefore, the modal change is made more apparent in that the chiseling and the increase in contact area resulted in a reduction of three-dimensional (twisting) behavior. Similar observations have been made with respect to ancient multi-drum columns, in which the elevated, outer bearing surfaces of the rocks were smoothened to increase resistance to lateral excitation.[23]

The modal results can further be summarized in the vector intensity domain as shown in Figure 7, which shows that the largest shift from rock-twist (RT) to rocking (R) occurs at lower values of PGA (i.e., PGA < 0.2 g). This indicates that the chiseling primarily impacts the low-amplitude responses, rather than the overturning. The implications of this are that precarious rock models should consider a full three-dimensional model across the vector intensity space, and utilization of low-amplitude cut-offs are not appropriate (e.g., PGA thresholds for inducing rocking).

3.4 | Repeatability

To explore the issue of repeatability, a total of 320 shake table tests were performed on Specimen 2 (SP2) by selecting 3 ground motions of different PGV/PGAs ranging from low to high—namely, 0.0288, 0.1044, and 0.15313 s. PGV/PGA is used to differentiate the motions based upon previous studies that have highlighted the relative importance of this intensity measure in predicting overturning behavior[20,21]; however, PGV/PGA does not uniquely determine overturning and results cannot necessarily be extrapolated to other motions. The repeatability tests aim to determine the PGA range, for each ground motion, that induces 0% overturning to 100% in successive repetitive trials. For this purpose, if a particular PGA does not result in overturning in 10 trials, the PGA is increased by a small increment. If even a single instance of

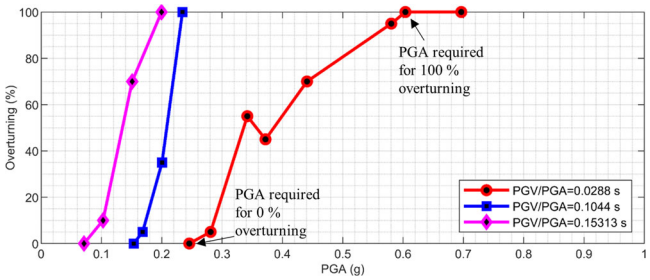

FIGURE 8 Repeatability tests results.

TABLE 2 Details of repeatability tests.

PGV/PGA (s)	PGA (0%)	PGA (100%)	PGA range	PGA Average	% variation
Low (0.0288)	0.245	0.604	0.36	0.425	42.17
Medium (0.1044)	0.153	0.234	0.08	0.194	20.86
High (0.15313)	0.071	0.20	0.129	0.135	47.50

overturning is observed in the next 10 trials of the PGA, 10 more repetitions (a total of 20) are done at the same PGA to provide a more reliable estimate of the overturning rate. Twenty tests are conducted at each incremental PGA until 100% overturning is achieved. The large number of trials at a given PGA are necessary given the sensitivity of the response due to even small changes in the original position of the specimen (angle of the excitation) or the input motion. Considerable effort was included to maintain consistency between tests, however, it is acknowledged that it is not feasible for all tests to be truly identical. It is also clarified that while the input signal is identical for each test at a given PGA, the achieved motion is still not entirely consistent. The shake table is operated via control of displacement, which is monitored for each test. Motion-to-motion variations in the displacement were primarily limited to small variations in peak displacements for motions at the same PGA, while small variations in frequency content were observed for scaled motions.

The overall results are shown in Figure 8, which plots the rate of overturning as a function of the incremental PGA for each of the ground motions. The results indicate that ground motions with lower PGV/PGA (i.e., higher frequency content) result in a large range of PGA demand as it shows that overturning can occur anywhere between 0.245 to 0.6 g (range of 0.355 g). On the other hand, a motion with high PGV/PGA (i.e., lower frequency content) shows a much smaller range. For these two high PGV/PGA ground motions, the PGA ranges are relatively small, 0.07 to 0.2 g (range of 0.13 g) and 0.15 to 0.24 g (range of 0.09 g). Table 2 presents these PGA ranges for each motion in terms of the percent variation from the average PGA demand for overturning. Despite the widely different ranges of PGA resulting in overturning, the percent variation from the average PGA demand varies much less with 20% variation for the ground motion with a medium PGV/PGA and 42% and 47% for the ground motions with low and high PGV/PGA. While this analysis indicates little reliance of the uncertainty on PGV/PGA, it still highlights that substantial uncertainty exist in the overturning. That is, the overturning demand can vary up to nearly ±50%.

As previously mentioned in Section 3.1, time histories of rigid body motion were acquired for these repeatability tests to further understand the uncertainty. It should be noted that in cases of overturning, the shake table is stopped prematurely to reduce impact to the specimen, which will be reflected in the time histories. A set of 6 tests consisting of 3 non overturning (NO) cases and 3 overturning (O) cases are selected at PGA levels in the center of the uncertainty range for each of the 3 ground motions to allow a deeper interpretation of the uncertainty. Figure 9A shows the in-plane displacement time histories of the rock for the high-frequency ground motion with PGV/PGA of 0.0288 s, while the corresponding rotations are shown in Figure 9B–D. It can be seen that the rock's response is in both in-plane (along ground motion direction) and out-of-plane which is due to the highly asymmetric geometry of both the rock and its base. However, the general response consists of a large number of small amplitude rocking cycles, as expected given the high-frequency motion. Regardless of whether the rock overturns or not, there are multiple impact events that are observed. In each case, twisting is observed to accumulate gradually in time. Each of these impact events and the accumulation of twist can have slight discrepancies in each trial that can lead to very different outcomes due to the significant non-linearities of the rigid body motion problem.

Figure 10 shows the displacement time histories of the rock and the shake table for the ground motion with a PGV/PGA of 0.1044 s, while Figure 10B–D shows corresponding rotations. It is evident that the rock's response is both in-plane

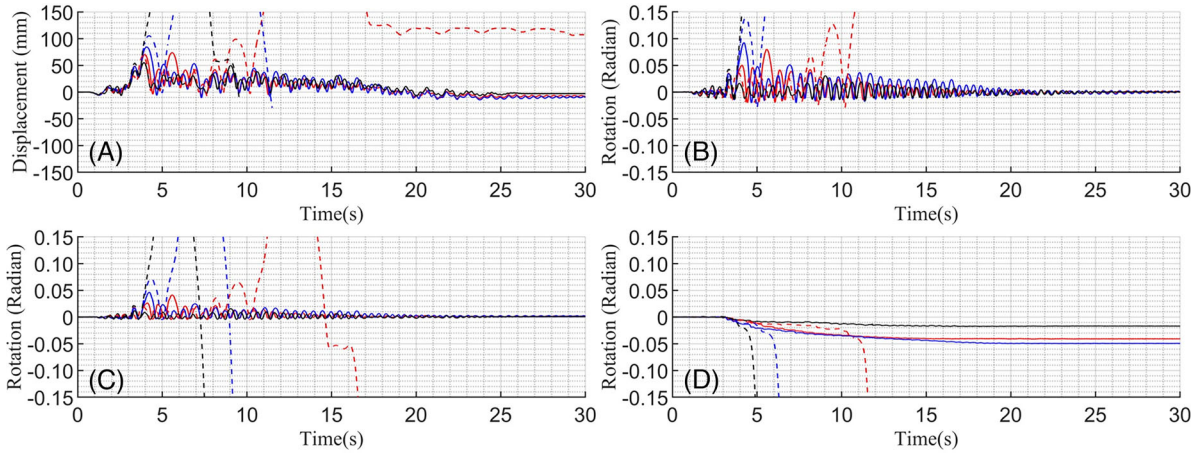

FIGURE 9 Response of rock with ground motion of PGV/PGA = 0.0288 s for six individual tests: (A) Displacement in the direction of motion, (B) in-plane rocking, (C) out-of-plane rocking, and (D) twisting.

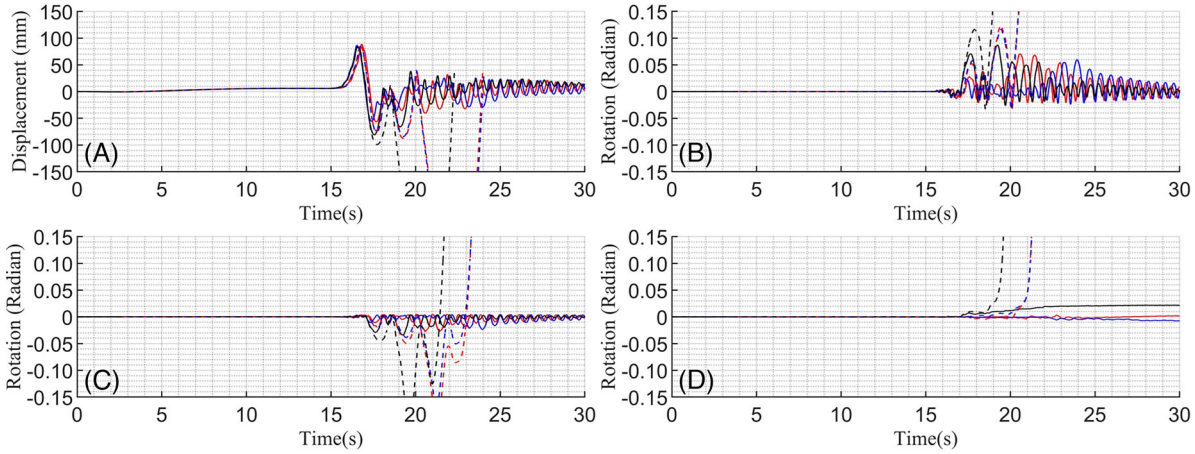

FIGURE 10 Response of rock with ground motion of PGV/PGA = 0.1044 s for six individual tests: (A) Displacement in the direction of motion, (B) in-plane rocking, (C) out-of-plane rocking, and (D) twisting.

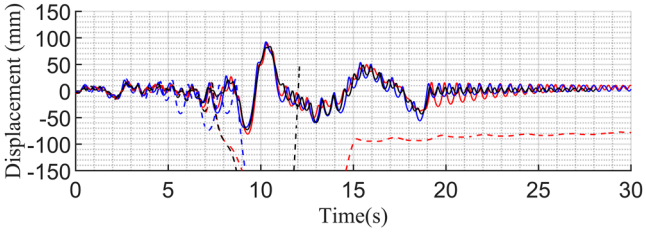

FIGURE 11 Displacement response of rock with ground motion of PGV/PGA = 0.15313 s for six individual tests.

(along ground motion direction) and out-of-plane. However, the general response consists of relatively large amplitude rocking cycles. Though one case (Case 3) shows some accumulation of twist, in general, the twist accumulation is minimal which is likely due to the rocking dominated response for this relatively low-frequency ground motion. Figure 11 shows the displacement response of the rock and the shake table for the ground motion with a PGV/PGA of 0.15313 s. Similar observations can be made from this figure as for the other low-frequency ground motion (i.e., the one with PGV/PGA of 0.1044 s) in that the response is dominated by large amplitude cycles. Rotation time histories are unable to be provided for this case, due to data acquisition failure; however, the key observations can still be made from the displacement histories.

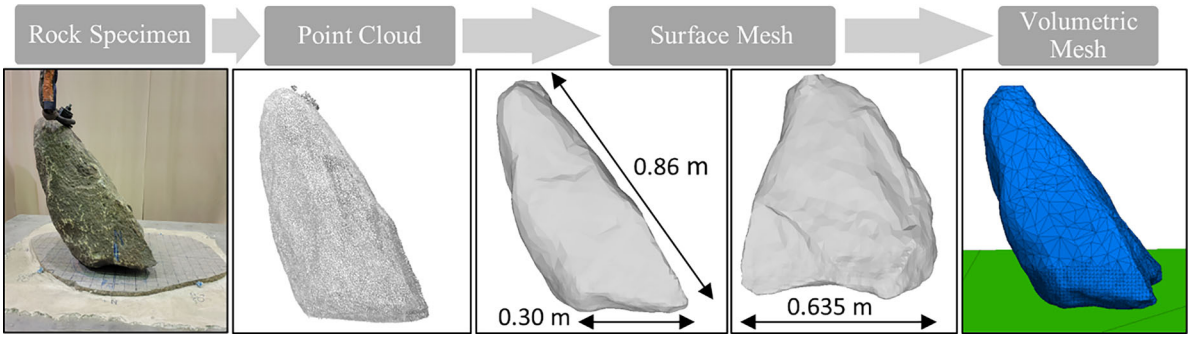

FIGURE 12 Steps involved in geometric modeling.

4 | NUMERICAL MODELING AND PARAMETRIC EVALUATION

Three-dimensional numerical modeling is an important tool to analyze the seismic response of freestanding structures. Though some studies shed light on the superiority of numerical modeling over two-dimensional analytical approaches, they also point toward the importance of certain contact/interface parameters (e.g., Saifullah and Wittich[12]), such as contact stiffness, to which the numerical seismic response may show sensitivity. This sensitivity is studied here for realistic and geometrically complex three-dimensional PBRs. Consequently, this section describes the geometric modeling process, the numerical modeling approach, and the effect of the variation in contact parameters (primarily normal stiffness) on the overturning response of the PBR specimens from the shake table testing campaign described in the previous section. Uncertainty in the numerical response is further evaluated with comparison to the experimental results. It is clarified that all simulations presented incorporated the achieved motions on the shake table, rather than the input signal.

4.1 | Geometric modeling

The geometric modeling process for the PBR specimens in this study is adopted from Saifullah and Wittich.[12] The numerical modeling of a geometrically complex freestanding structure such as PBR is done by utilizing lidar scans. Multiple scans of the granite specimen were taken before the start of testing to reduce occlusion, which are registered to a common coordinate system to form a single point cloud. A surface mesh is then generated in MeshLab[24] by using Poisson Surface Reconstruction (PSR).[25] Previous studies that have employed this algorithm (e.g., Wittich et al.,[26] Ducke et al.,[27] D'Altri et al.,[28] Saifullah and Wittich[12]) suggest that the adopted algorithm is the optimal choice for a watertight mesh for complex geometries with sharp gradients since it considers the entire data set at once and inherently filters surface noise by fitting a function to the surface.[25] This surface mesh is then converted into a volumetric mesh in a numerical distinct element method based program, 3DEC, which is explained in the next subsection. A flow chart summarizing the process of geometric modeling is shown in Figure 12. This process can yield extremely fine meshes, which is one of the primary justifications for its usage; however, this can also result in very large files and run times. For this reason, the mesh of the rock was simplified for the upper part of the rock only (i.e., that which would not be reasonably expected to interact with the pedestal below). A very fine mesh was maintained at the interface.

4.2 | Distinct element method and modeling

The PBR specimens are numerically simulated using the distinct element method. The distinct element method is a subclass of Discrete Element Codes that provides the capability of representing the motion of multiple intersecting discontinuities explicitly, thus offering the attractiveness of adequate representation of failure modes (rocking, sliding, overturning, etc.) for freestanding structures. It employs an efficient algorithm for detecting and classifying contacts and uses an explicit time-marching scheme to solve the equations of motion directly. The contacts are treated as deformable contacts while the bodies can be modeled as rigid or deformable. This method was first introduced by Cundall in 1971,[29,30] and is now available in both two-dimensional and three-dimensional codes, UDEC[31] and 3DEC.[32]

TABLE 3 Contact model parameters.

Model parameter	Value
Normal stiffness (K_N)	3, 5, 10, 15, 20 GPa/m
Shear stiffness (K_S)	1 GPa/m
Friction angle (ϕ)	40°
Tensile strength	0 MPa
Cohesion	0 MPa
Damping	0

The efficiency of the contact detection scheme emanates from the common-plane logic that defines the sliding plane between the two interacting blocks. This imaginary common-plane is analogous to a metal plate which can become trapped and may become deflected by the intersecting blocks. All types of interactions, including face-to-face interactions, are simulated through two primary contact types, that is, vertex-to-face and edge-to-edge contacts. Subcontacts are formed at the vertices by triangulating the faces, which are then used to monitor interaction forces, sliding, separation, etc. Each subcontact is assigned an area equal to one-third of the area of the surrounding triangles. The contact/interface of two interacting blocks are represented with two sets of parallel springs, the contact forces from these two sets are averaged to obtain the overall interface behavior. A typical calculation cycle involves the application of Newton's second law of motion and the constitutive relationship. The constitutive law that is adopted for the joint behavior in this study is the Columb slip model, as it provides a linear representation of joint stiffness and yield limit. The Coulomb model uses elastic stiffness, frictional, cohesive strength, tensile strength, and dilation angle, while considering both tensile and shear failures. The joint forces are dependent on the elastic contact stiffnesses,[10,11] K_N and K_S, contact area, A_c, and the relative displacements (as shown in Equations 1 and 2), ΔU_N and ΔU_S, where the former is defined by the user and the latter is measured by tracking subcontact displacement on one face and subtracting the displacement of coincident sub-contact on the other interacting face. It is clarified that these equations are valid only for the elastic step, prior to violation of the Coulomb law. Additional details on the joint model can be found in the original paper by Hart et al.[33] and in the supporting literature of Itasca 3DEC[31]

$$\Delta F_N = K_N \, \Delta U_N A_C \tag{1}$$

$$\Delta F_S = K_S \, \Delta U_S A_C \tag{2}$$

The distinct element modeling of the rock specimens is accomplished in 3DEC.[32] The rock geometry is modeled by importing the surface mesh into 3DEC and assigning a mass density of 2750 kg/m^3 (for granite) to convert into a volumetric model. A rectangular pedestal is modeled with the same material to emulate the granite slab and the shake table, on which the rock is supported and to which the earthquake input is applied. It is noted that the input excitations to the model are the achieved ground motions from the shake table testing. The behavior of these structures is governed by the relative movement of the interacting blocks, therefore rigid material is a reasonable assumption for these structures as demonstrated by Psycharis et al.[10] Both the rock and the pedestal are modeled as rigid with deformation existing only at the rock-pedestal joint/interface. The current study assumes that the tensile strength of the joint in the normal direction is zero. This is a realistic assumption due to freestanding nature of the rock with the joint comprised of compression-only springs. Moreover, the contribution of cohesion to the shear strength of the joints is not taken into consideration and the shear strength is governed by the friction angle. While it is acknowledged that damping is known to significantly alter the response of systems modeled via DEM, damping is taken as zero herein, based upon previous studies which demonstrated satisfactory results during strong ground motion excitation.[9,34,35] Normal stiffness is the main parameter influencing the response; therefore, multiple values are incorporated and compared, as listed in Table 3.

4.3 | Results and discussion

The results obtained from shake table experimentation and the numerical analyses are presented and analyzed in two ways. First, the raw results are analyzed to aid in initial interpretation and to identify optimal numerical modeling

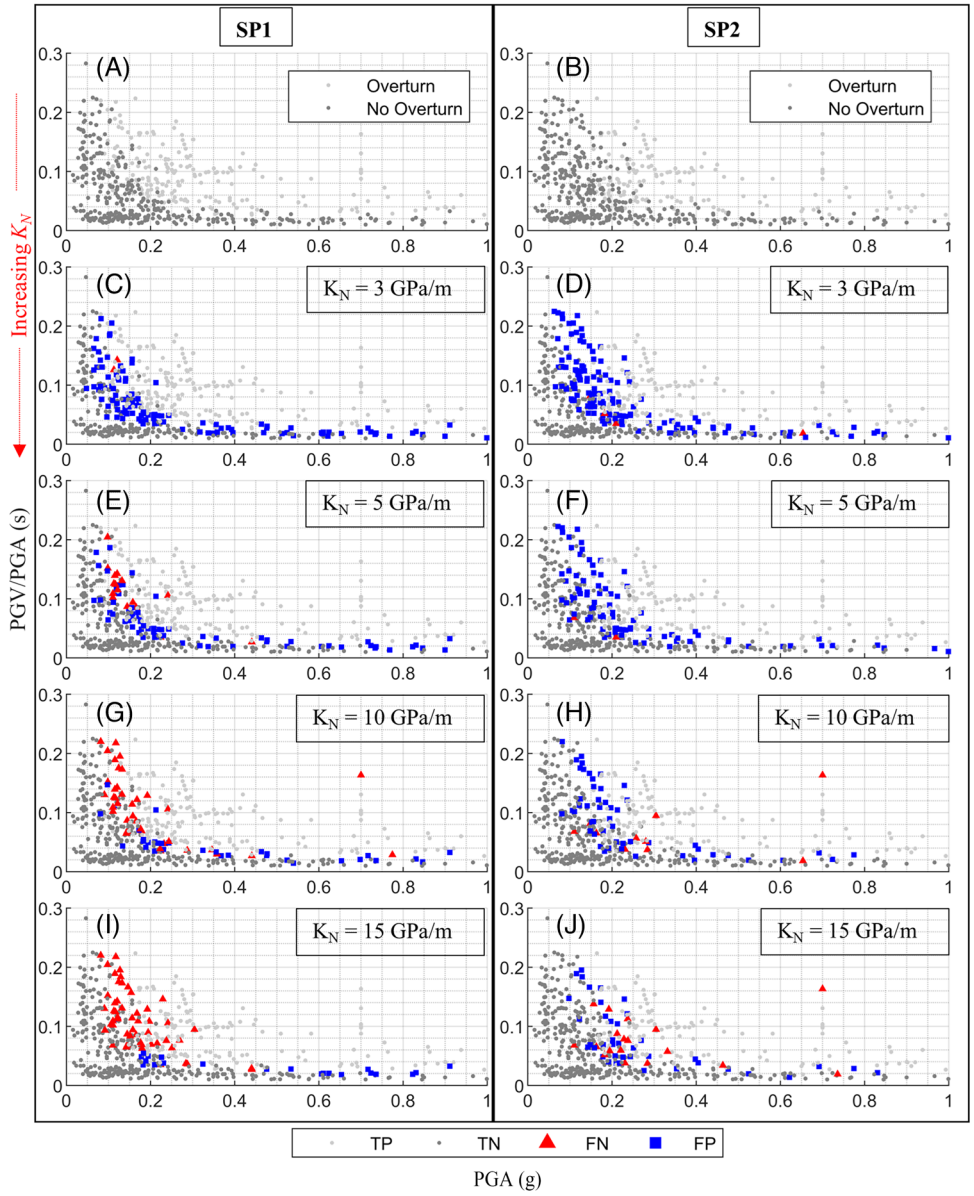

FIGURE 13 Raw data comparison. (A) Experimental SP1, (B) Experimental SP2, (C) SP1 3 GPa/m, (D) SP2 3 GPa/m, (E) SP1 5 GPa/m, (F) SP2 5 GPa/m, (G) SP1 10 GPa/m, (H) SP2 10 GPa/m, and (I) SP1 15 GPa/m.

parameters. This is followed by a probabilistic comparison to aid in trend identification. The results are presented in the following sub-sections, as organized by the key parameter being investigated and the use of the raw or probabilistic data. All numerical analyses utilized the achieved shake table motions and not the input signal.

4.3.1 | Normal stiffness

The raw numerical results for both the unchiseled specimen (SP1) and the chiseled (SP2) are presented in Figure 13. The top row of this figure (Figure 13A,B) shows the experimental results of SP1 and SP2 in terms of overturning (light gray) and non-overturning (dark gray) in PGA-PGV/PGA space. Below each of the specimen's experimental results is a column of numerical results with variation of the normal stiffness K_N. The numerical results are presented as the outcome of a binary classification problem (overturning or non-overturning), in which the experimental results are treated as the ground truth. That is, each simulation result is classified as: true positive (TP), true negative (TN), false negative (FN), or false positive (FP). For a particular specimen (SP1 or SP2), if the numerical prediction agrees with the experimental result

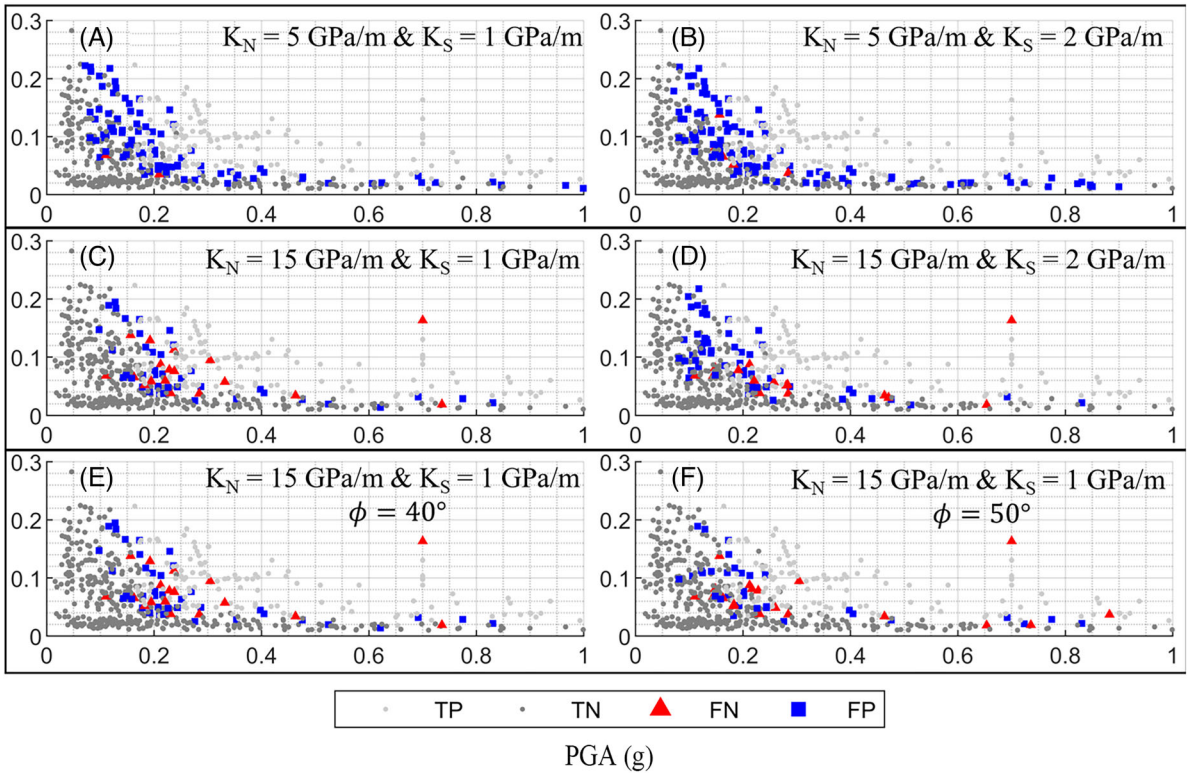

FIGURE 14 Raw data comparison (A) $K_N = 5$ GPa/m, $K_S = 1$ GPa/m, (B) $K_N = 5$ GPa/m, $K_S = 2$ GPa/m, (C) $K_N = 15$ GPa/m, $K_S = 1$ GPa/m, (D) $K_N = 15$ GPa/m, $K_S = 2$ GPa/m, (E) $K_N = 15$ GPa/m, $K_S = 1$ GPa/m, $\phi = 40°$, (F) $K_N = 15$ GPa/m, $K_S = 1$ GPa/m, $\phi = 50°$.

in terms of overturning (O), it is as true positive (TP), whereas, it would be labeled true negative (TN) if the numerical prediction agrees with the experimental result non-overturning (NO). Likewise, a numerical prediction is labeled as a false negative (FN) when the prediction yields non-overturning (NO) and contradicts the experimental result of overturning. False positive (FP) occurs when the numerical prediction is overturning (O) and contradicts the experimental result of non-overturning (NO).

From Figure 13, it can be seen that for both SP1 and SP2, with the increase in normal stiffness, the number of false positive (FP) cases decreases, while the number of false negative (FN) cases increases. This indicates that the model becomes less conservative at higher values of normal stiffness. It also shows that for the same stiffness values (comparing within the same row of Figure 13), the chiseled specimen (SP2) has more instances of false positives (FP) compared to the unchiseled specimen (SP1), which as more instances of false negatives. This may be arising due to the relatively flatter base of the SP2 rock which is able to establish more contact points. This increase in contact points results in larger contact forces and an increase in rocking motion.

4.3.2 | Other contact parameters

In order to briefly assess the impact of shear stiffness K_S, and the friction angle ϕ, numerical results of the chiseled specimen (SP2) considering variations of these parameters are presented in Figure 14. Figure 14A,B shows how the TP, FP, TN, FN cases vary when the shear stiffness K_S is changed from 1 to 2 GPa/m while keeping the normal stiffness K_N as 5 GPa/m. Similarly, Figure 14C,D shows the results when the normal stiffness K_N is kept as 15 GPa/m while the shear stiffness K_S is changed from 1 to 2 GPa/m. In both these cases, an increase of false positive (FP) cases is noted as the shear stiffness is increased from 1 to 2 GPa/m. Figure 14E,F shows the effect of changing the friction angle ϕ from 40° to 50° while keeping the K_N and K_S fixed at 15 and 1 GPa/m, respectively. In each case, a difference in the false positives is observed. While differences can be observed in each comparison presented in Figure 14 with respect to changes in shear stiffness and friction angle, the differences are relatively small in comparison to those introduced by the normal stiffness.

TABLE 4 Scoring metrics of different numerical models.

Numerical model	Accuracy	Precision	Recall	F1 score
SP1– $K_N = 3$, $K_S = 1$	0.798969	0.677966	0.987654	0.804020
SP1– $K_N = 5$, $K_S = 1$	0.852234	0.766102	0.930041	0.840149
SP1– $K_N = 10$, $K_S = 1$	0.872852	0.853556	0.839506	0.846473
SP1– $K_N = 15$, $K_S = 1$	0.869416	0.888372	0.786008	0.834061
SP2– $K_N = 3$, $K_S = 1$	0.747423	0.569697	0.974093	0.718929
SP2– $K_N = 5$, $K_S = 1$	0.836770	0.673759	0.984456	0.800000
SP2– $K_N = 10$, $K_S = 1$	0.886598	0.777293	0.922280	0.843602
SP2– $K_N = 15$, $K_S = 1$	0.895189	0.808411	0.896373	0.850123
SP2– $K_N = 20$, $K_S = 1$	0.883162	0.830688	0.813472	0.821990
SP2– $K_N = 15$, $K_S = 2$	0.867698	0.750000	0.901554	0.818824
SP2– $K_N = 15$, $K_S = 1$, $\phi = 50^\circ$	0.902062	0.830097	0.886010	0.857143
SP2– $K_N = 5$, $K_S = 2$	0.807560	0.639175	0.963731	0.768595

4.3.3 | Model performance

Despite the nuances in model performance in Figures 13 and 14, the models appear to perform quite well across the parameter ranges for both specimens. To assess which models perform best, Table 4 presents four metrics for each model, which are defined below. For each specimen, the best performing models are highlighted in red.

- **Accuracy** represents the number of correctly predicted/classified cases and is given by the following formula

$$Accuracy = \frac{TP + TN}{Total\ (TP + TN + FP + FN)}$$

- **Precision** is the ratio of correctly predicted positive observations to the total predicted positive observations and is given by the following formula

$$Precision = \frac{TP}{TP + FP}$$

- **Recall** is the ratio of correctly predicted positive observations to all observations in actual positive class and is given by the following formula

$$Recall = \frac{TP}{TP + FN}$$

- **F1 Score** is the weighted average of precision and recall and therefore takes both into account. It is generally considered a better classification measure if there is an uneven class distribution and is given by the following formula

$$F1\ Score = 2 \times \frac{Precision \times Recall}{Precision + Recall}$$

In Table 4, it is shown that the accuracy and F1 score are better for the chiseled model (SP2) as compared to the unchiseled model (SP1). This likely results from the relatively simpler interface geometry of SP2, which is better approximated by the geometry of the numerical model. The highest accuracy and F1 score that is achieved for SP1 are in the case with $K_N = 10$ GPa/m, $K_S = 1$ GPa/m. With further increase in normal stiffness (i.e., $K_N = 10$ GPa/m, $K_S = 1$ GPa/m), the accuracy and the F1 score decrease. Similarly, for the SP2 model, the highest accuracy and F1 score are obtained with $K_N = 15$ GPa/m, $K_S = 1$ GPa/m, while the accuracy and the F1 score decrease with further increase in normal stiffness (i.e., $K_N = 20$ GPa/m, $K_S = 1$ GPa/m). A slightly better F1 score and accuracy for SP2 is obtained by increasing the friction angle from 40° to 50°,

however, the difference is not significant (less than 1% increase). Table 4 also shows that increase in shear stiffness from $K_S = 1$ GPa/m to $K_S = 2$ GPa/m results in a decrease in accuracy and the F1 score, which aligns with the observations made in Figure 14. While the optimal model parameters differ for SP1 and SP2, there is relatively little difference in the model performance considering normal stiffnesses from 5 to 15 GPa/m.

4.3.4 | Probabilistic analysis

As mentioned in the introduction, it is important to analyze the results in the probabilistic domain to aid in trend identification. To achieve this, a vector-valued fragility analysis is conducted to assess the uncertainty associated with the changes at the interface (i.e., unchiseled, and chiseled versions) and the contact stiffness. Vector-valued ground motion intensity measures (i.e., PGA and PGV/PGA) are used to assess the overturning results in probabilistic format. For problems with binary outcomes, logistic regression is deemed as the most suitable choice to develop fragilities. Since the response quantity in the current study is dichotomous and alternates between two forms, overturning and no overturning, logistic regression is adopted. The probability of overturning is obtained by using Equation (3).

$$P\left(\text{Overturning}|\ x_1 = \text{PGA},\ x_2 = \frac{\text{PGV}}{\text{PGA}}\right) = \frac{1}{1 + e^{-(\beta_0 + \beta_1 x_1)}} \tag{3}$$

where P indicates the probability of overturning, while β_0 and β_1 are the regression coefficients corresponding to intercept and slope. The data is initially binned based on PGV/PGA and the regression is performed as a function of PGA for each bin. The resulting fragilities are placed at the median value of PGV/PGA of each bin, which is then converted into fragility surfaces. Due to the difficulty of directly comparing these fragility surfaces with each other, fragility contours at different probability levels are compared, which is why only an example fragility surface is shown in Figure 15A for conciseness. In the current case, the fragility contours at 10% probability, 50% probability, and 95% probability of overturning (marked on the fragility surface in Figure 15A) are compared and analyzed in Figure 15B–D respectively.

The experimental fragility contours for all probability levels highlight the increased stability of SP2 compared to SP1 (Figure 15B–D). Considering the 10% probability contour (Figure 15B), at PGV/PGA of 0.11 s, the PGA demand for SP1 and SP2 are 0.075 and 0.165 g, respectively, which indicates that the intensity (PGA) demand for overturning for SP2 is more than 200% of the demand for SP1. This difference is present at PGV/PGAs starting at 0.08 s and above. Similarly, at 50% probability level (Figure 15C), the intensity demand for SP1 (unchiseled) and SP2 (chiseled) at PGV/PGA of 0.11 s is 0.135 and 0.21 g, respectively. This difference translates to more than 150% of the intensity (PGA) demand for SP2 than required for SP1, and this difference remains similar at higher values of PGV/PGA. While slightly less pronounced, a similar trend can be observed at the highest probability level (Figure 15D). While the difference in the interface geometry between SP1 and SP2 is minimal, this is a stark difference in demand, or increase in stability, arising from the chiseling of the specimen. This emphasizes the potential impact of interface assumptions or measurements during field surveying of PBRs. Furthermore, the difference between the specimens is diminished at very low levels of PGV/PGA. This is likely due to the low instances of overturning due to these high-frequency motions.

Considering the fragility contours of the numerical models, it can be seen that for both SP1 (unchiseled) and SP2 (chiseled) numerical models, the increase in normal stiffness results in more stable model and reduced overturning (i.e., the intensity demand for overturning increases). Looking more closely, SP1 (unchiseled) models tend to show a wider range of uncertainty compared with those of SP2 (chiseled). For example, considering the 10% probability contour and a PGV/PGA of 0.11 s, the intensity demand varies from 0.025 g (with $K_N = 3$ GPa/m model) to 0.15 g (with $K_N = 15$ GPa/m model) for SP1, whereas this range varies from 0.05 g (with $K_N = 3$ GPa/m & $K_N = 3$ GPa/m models) to 0.13 g (with $K_N = 15$ GPa/m model) for SP2 (Figure 15B). This could be explained in terms of chiseling of the interface, where the smoothened base of SP2 is able to establish more contact points as compared to the corresponding SP1 model and thus contributing to comparably reduced variation in results as the stiffness is increased. Nevertheless, SP2 (chiseled) fragility contour range is unable to fully envelop/contain the experimental SP2 (chiseled) fragility contour at all probability levels, while SP1 (unchiseled) fragility contour range is able to do so. While other combinations of model parameters could potentially contribute to better performance, it is likely that this difference results from the probabilistic approach itself and the number of overturning instances. It is emphasized that the model performance

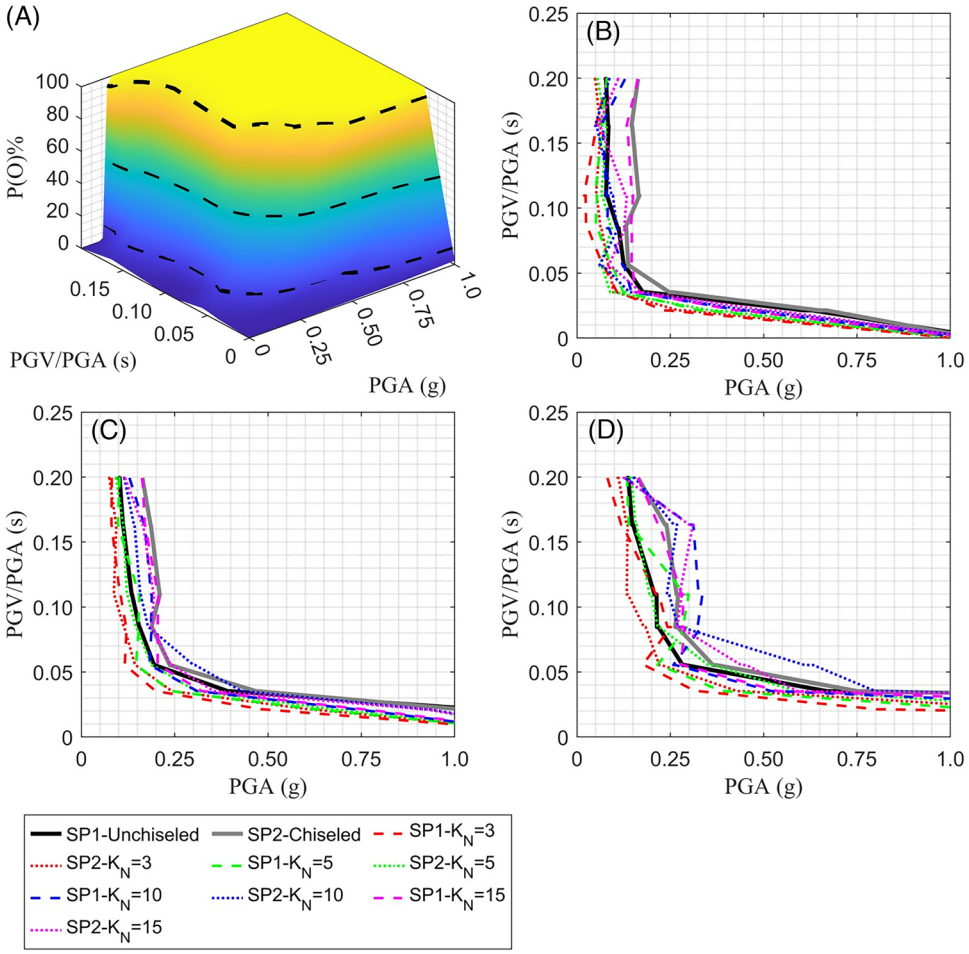

FIGURE 15 Probabilistic analyses. (A) Sample fragility surface, (B) fragility contours at 10% probability of overturning, (C) fragility contours at 50% probability of overturning, and (D) fragility contours at 95% probability of overturning.

was evaluated in Table 4, which shows comparable and strong predictive abilities of the numerical models for both specimens.

4.3.5 | Other contact parameters

This subsection touches upon the influence of other contact parameters, such as shear stiffness and friction angle. Figure 16A–C shows the fragility contours for the cases of SP2 (chiseled) where the shear stiffness K_S is increased from 1 to 2 GPa/m and one case where friction angle ϕ is increased from 40° to 50°. It is noted that for all numerical models, friction angle is ϕ is fixed to 40°. In addition, an additional case with $K_N = 20$ GPa/m is presented at 10% probability level, for the large part of the fragility contours, the increase in shear stiffness results in a decrease in PGA demand (i.e., the model becomes more fragile). The numerical case with $K_N = 20$ GPa/m does approach the experimental contour for SP2 at PGV/PGA less than 0.04 s, however, it still fails to approach the experimental fragility SP2 at PGV/PGA higher than 0.04 s.

At 50% probability of overturning (Figure 16B), the change in shear stiffness from 1 to 2 GPa/m with $K_N = 5$ GPa/m does not result in a substantial difference among the contours of these models. The difference is much more pronounced for model with $K_N = 15$ GPa/m where the shear stiffness increases from 1 to 2 GPa/m results in large differences in PGA demand at PGV/PGA higher than 0.06 s. The increase in friction angle also indicates an increase in stability as the PGA demand, in general, is higher with $\phi = 50°$ compared to the case where $\phi = 40°$. At 95% probability of overturning (Figure 16C), the contours with $K_N = 20$ GPa/m shows a large deviation from $K_N = 15$ GPa/m for PGV/PGA less than

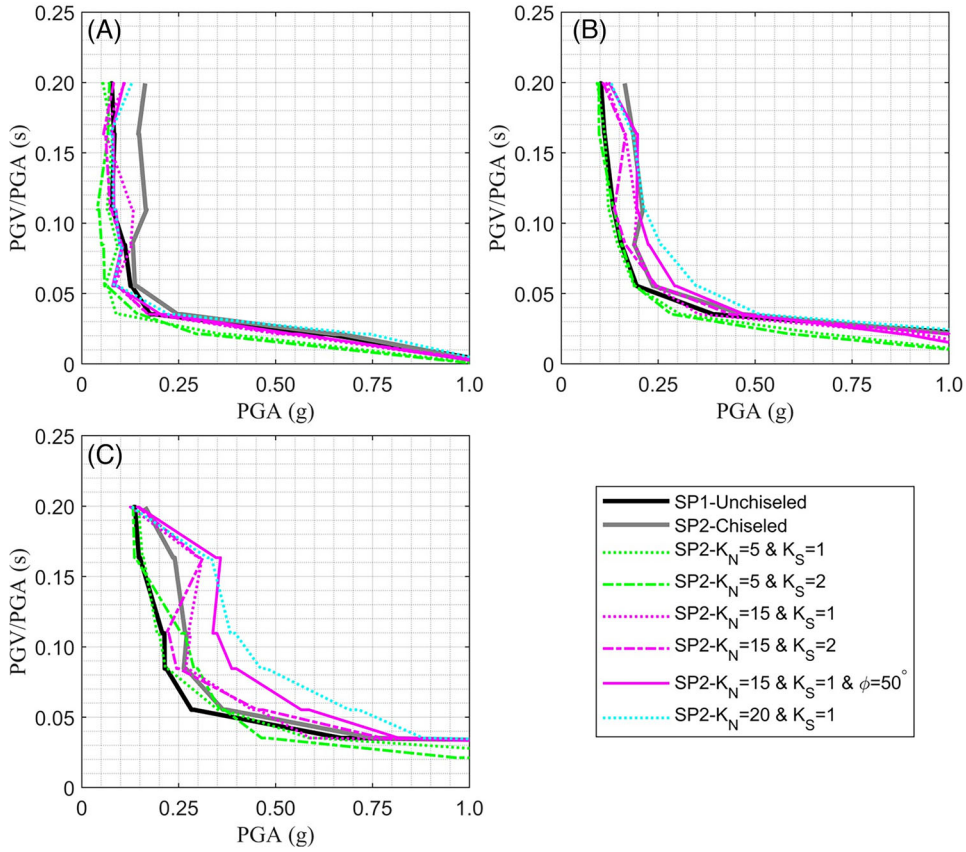

FIGURE 16 Probabilistic Analyses for other parameters. (A) Fragility contours at 10% probability of overturning, (B) fragility contours at 50% probability of overturning, and (C) fragility contours at 95% probability of overturning.

0.10 s. The case with friction angle $\phi = 50°$ also shows increased stability, however, this increase in PGA demand is not as large as the one observed with increasing normal stiffness to $K_N = 20$ GPa.

5 | CONCLUSION

This study investigates the effects of physical and numerical parameter changes on the uncertainty of granitic rock specimens, which are considered representations of PBRs. Shake table tests are conducted on an unchiseled specimen, and the same specimen is then chiseled to introduce small changes at the interface and tested again with the same protocol. With smoothening of the interface without measurable changes in the overall rock geometry, there is a large shift in dominant modes of response from rock-twist to rocking. The results indicate that a small variation in the contact geometry could result in a substantial increase in the stability of the specimen (i.e., at some probability levels more than 200% increase in PGA demand), which is significant given the difficulty of surveying the interface of PBRs in the field. The repeatability tests on the specimen indicate that low PGV/PGA ground motions show a wide range of PGA demand, where overturning was observed to occur over a PGA range in excess of 0.3 g. The percent error with respect to an average demand ranges from approximately 20% to 47%, with little apparent relation to the PGV/PGA. While PGV/PGA is commonly utilized within PBR analyses and for other freestanding structures, this intensity measure does not uniquely determine overturning, and care should be taken to extrapolate these results to other ground motions. Furthermore, the geometrically complex specimen was subjected to uniaxial excitation and different results would be expected under biaxial excitations or even if the excitation angle were to change. Despite these limitations, this study still highlights that substantial uncertainty may exist in the overturning. That is, the overturning demand can vary up to nearly ±50%, however, this uncertainty still inherently accounts for the repeatability of the experimental setup and true uncertainty may be lower.

Furthermore, the specimens are modeled on a distinct element method program to study the influence of contact stiffness on the overturning response. Numerical results reveal that the chiseled specimen models perform better than the

unchiseled ones due to the model geometry being able to more closely replicate the smoother interface. The optimal numerical model for the unchiseled specimen considers a normal stiffness of 10 GPa/m and shear stiffness of 1 GPa/m, while values of 15 GPa/m and 1 GPa/m for the normal and shear stiffnesses, respectively, are needed for the chiseled specimen. Despite the difference in optimal models, there is relatively little difference in the performance of models considering normal stiffnesses within the range of 5–15 GPa/m. The results start diverging from the experimental baseline beyond these values, which shows that the stability of the rock can be overestimated due to model parameter selection. In general, though, a high contact stiffness in the range of 10—15 GPa/m performs much better than values less than 5 GPa/m.

ACKNOWLEDGMENTS

Funding for this research was provided, in part, by the Southern California Earthquake Center (SCEC), under SCEC Award #20106, and by Pacific Gas and Electric Company (PG&E). SCEC is funded by National Science Foundation Cooperative Agreement EAR-1600087 and United States Geological Survey Cooperative Agreement G17AC00047. The numerical simulations were completed using the Holland Computing Center of the University of Nebraska, which receives support from the Nebraska Research Initiative. The authors also extend their gratitude for the physical assistance of Mr. Peter Hilsabeck (Structures Laboratory Manager) and Mr. Ben Gomen (Structures Laboratory Assistant) as well as numerous undergraduate assistants at the shake table including Ms. Nicole Fiebiger, Mr. Trystan Hymes, and Mr. Nick Kleinschmidt.

DATA AVAILABILITY STATEMENT

The data that support the findings of this study are available from the corresponding author upon reasonable request.

ORCID

Christine E. Wittich https://orcid.org/0000-0002-2678-7310

REFERENCES

1. Housner GW. The behavior of inverted pendulum structures during earthquakes. *Bull Seismol Soc Am*. 1963;53(2):403-417.
2. Yim C-S, Chopra AK, Penzien J. Rocking response of rigid blocks to earthquakes. *Earthq Eng Struct Dyn*. 1980;8(6):565-587. doi:10.1002/eqe.4290080606
3. Peña F, Prieto F, Lourenço PB, Costa AC, Lemos JV. On the dynamics of rocking motion of single rigid-block structures. *Earthq Eng Struct Dyn*. 2007;36(15):2383-2399. doi:10.1002/eqe.739
4. Psycharis IN, Jennings PC. Rocking of slender rigid bodies allowed to uplift. *Earthq Eng Struct Dyn*. 1983;11(1):57-76. doi:10.1002/eqe.4290110106
5. Ishiyama Y. Motions of rigid bodies and criteria for overturning by earthquake excitations. *Earthq Eng Struct Dyn*. 1982;10(5):635-650. doi:10.1002/eqe.4290100502
6. Shenton HW, Jones NP. Base excitation of rigid bodies. I: formulation. *J Eng Mech*. 1991;117(10):2286-2306. doi:10.1061/(asce)0733-9399(1991)117:10(2286)
7. Konstantinidis D, Makris N, The dynamics of a rocking block in three dimensions. 8th HSTAM International Congress on Mechanics, Patras, Greece, 2007.
8. Chatzis MN, Smyth AW. Modeling of the 3D rocking problem. *Int J Non Linear Mech*. 2012;47(4):85-98. doi:10.1016/j.ijnonlinmec.2012.02.004
9. Papantonopoulos C, Psycharis IN, Papastamatiou DY, Lemos JV, Mouzakis HP. Numerical prediction of the earthquake response of classical columns using the distinct element method. *Earthq Eng Struct Dyn*. 2002;31(9):1699-1717. doi:10.1002/eqe.185
10. Psycharis IN, Lemos JV, Papastamatiou DY, Zambas C, Papantonopoulos C. Numerical study of the seismic behaviour of a part of the Parthenon Pronaos. *Earthq Eng Struct Dyn*. 2003;32(13):2063-2084. doi:10.1002/eqe.315
11. Ambraseys N, Psycharis IN. Earthquake stability of columns and statues. *J Earthq Eng*. 2011;15(5):685-710. doi:10.1080/13632469.2010.541549
12. Saifullah MK, Wittich CE. Seismic response of two freestanding statue-pedestal systems during the 2014 South Napa earthquake. *J Earthq Eng*. 2021;26:5086-5108. doi:10.1080/13632469.2020.1859004
13. Mouzakis HP, Psycharis IN, Papastamatiou DY, Carydis PG, Papantonopoulos C, Zambas C. Experimental investigation of the earthquake response of a model of a marble classical column. *Earthq Eng Struct Dyn*. 2002;31(9):1681-1698. doi:10.1002/eqe.184
14. Mathey C, Feau C, Politopoulos I, Clair D, Baillet L, Fogli M. Behavior of rigid blocks with geometrical defects under seismic motion: an experimental and numerical study. *Earthq Eng Struct Dyn*. 2016;45(15):2455-2474. doi:10.1002/eqe.2773
15. ElGawady MA, Ma Q, Butterworth JW, Ingham J. Effects of interface material on the performance of free rocking blocks. *Earthq Eng Struct Dyn*. 2011;40(4):375-392. doi:10.1002/eqe.1025
16. Purvance MD, Anooshehpoor A, Brune JN. Freestanding block overturning fragilities: numerical simulation and experimental validation. *Earthq Eng Struct Dyn*. 2008;37(5):791-808. doi:10.1002/eqe.789
17. Wittich CE, Hutchinson TC, DeSanto J, Sandwell D, 3-D reconstructions and numerical simulations of precarious rocks in Southern California. 11th National Conference on Earthquake engineering. Los Angeles, California, 2018.

18. Ancheta TD, Darragh RB, Stewart JP, et al. *PEER NGA-West2 Database*, Technical Report PEER 2013/03. Pacific Earthquake Engineering Research; 2013.
19. Center for Engineering Strong Motion Data. *Lamjung, Nepal Earthquake of 25 April 2015*. CESMD. 2015. https://strongmotioncenter.org
20. Purvance MD. *Overturning of Slender Blocks: Numerical Investigation and Application to Precariously Balanced Rocks in Southern California*. Ph.D. dissertation. Department of Geological Sciences, University of Nevada; 2005.
21. Dimitrakapolous EG, Paraskeva TS. Dimensionless fragility curves for rocking response to near-fault excitations. *Earthq Eng Struct Dyn*. 2015;44(12):2015-2033.
22. CloudCompare (version 2.10.3) [GPL software]. 2021. http://www.cloudcompare.org/
23. Sapirstein P, Psota E. Pattern matching and the analysis of damaged ancient objects: the case of the column drum. *J Comput Cult Heritage*. 2016;9(3):1-22.
24. Cignoni P, Callieri M, Corsini M, Dellepiane M, Ganovelli F, Ranzuglia G, MeshLab: an open-source mesh processing tool. Proc. of the Sixth Eurographics Italian Chapter Conference, Salerno, Italy, pp. 129-136, 2008.
25. Kazhdan M, Bolitho M, Hoppe H, Poisson surface reconstruction. Proc. of the 4th Eurographics Symposium on Geometry Processing, Aire-la-Ville, Switzerland, pp. 61-70, 2006.
26. Wittich CE, Hutchinson TC, Wood RL, Seracini M, Kuester F. Characterization of full-scale, human-form, culturally important statues: case study. *J Comput Civil Eng*. 2016;30(3). doi:10.1061/(asce)cp.1943-5487.0000508
27. Ducke B, Score D, Reeves J. Multiview 3D reconstruction of the archaeological site at Weymouth from image series. *Comput Graphics*. 2011;35(2):375-382. doi:10.1016/j.cag.2011.01.006
28. D'Altri AM, Milani G, de Miranda S, Castellazzi G, Sarhosis V. In: Aguilar R, Torrealva D, Moreira S, Pando MA, Ramos LF, eds. *On the Stability Analysis of a Geometrically Complex Leaning Historic Structure in Structural Analysis of Historical Constructions*. Springer, Cham; 2019:975-982.
29. Cundall PA, A computer model for simulating progressive, large-scale movements in blocky rock systems. Proceedings of the International Symposium on Rock Mechanics, Nancy, France, 1971;2(8):129-136
30. Cundall PA, Strack ODL. A discrete numerical model for granular assemblies. *Géotechnique*. 1979;29(1):47-65. doi:10.1680/geot.1979.29.1.47
31. Itasca Consulting Group. *Inc. UDEC — Universal Distinct Element Code. Theory and Background*. Itasca Consulting Group; 2004.
32. Itasca Consulting Group. *Inc. 3DEC — Three-Dimensional Distinct Element Code*. Itasca Consulting Group; 2016; Ver. 5.2.
33. Hart R, Cundall PA, Lemos J. Formulation of a three-dimensional distinct element model – Part II. Mechanical calculations for motion and interaction of a system composed of many polyhedral blocks. *Int J Rock Mech Min Sci Geomech*. 1988;25(3):117-125. doi:10.1016/0148-9062(88)92294-2
34. Psycharis IN, Papastamatiou DY, Alexandris AP. Parametric investigation of the stability of classical columns under harmonic and earthquake excitations. *Earthq Eng Struct Dyn*. 2000;29(8):1093-1109.
35. Ambraseys N, Psycharis IN. Assessment of the long-term seismicity of Athens from two classical columns. *Bull Earthq Eng*. 2012;10(6):1635-1666.

How to cite this article: Saifullah MK, Wittich CE. Uncertainty in overturning of precariously balanced rocks due to basal contact. *Earthquake Engng Struct Dyn*. 2023;1-20. https://doi.org/10.1002/eqe.3970